IEEE Access
Multidisciplinary | Rapid Review | Open Access Journal

Date of publication xxxx 00, 0000, date of current version xxxx 00, 0000.

Digital Object Identifier 10.1109/ACCESS.2022.Doi Number

Response Analysis of a Piezoelectric Ceramic Transducer Pair Excited by Phase-modulated Signals for Improved Echo Measurement

Přemysl Janů[1], Pavel Dyčka[1], Josef Bajer[1], Radek Bystřický[1], Barbora Odvárková[2]

[1]Department of Aviation Technology, Faculty of Military Technology, University of Defence, Kounicova 65, 66210, Brno, Czech Republic
[2]Department of Communication Technologies, Electronic Warfare and Radiolocation, Faculty of Military Technology, University of Defence, Kounicova 65, 66210, Brno, Czech Republic

Corresponding author: Přemysl Janů (e-mail: premysl.janu@unob.cz).

The work presented in this article was supported by the Czech Republic Ministry of Defence – University of Defence Development Program – "Conduction of Operations in Airspace", the Czech Republic Ministry of Education, Youth and Sports – University of Defence student research program "Modern Methods of Generation, Direction Control and Signal Processing" and the Czech Republic Ministry of Education, Youth and Sports – University of Defence student research program "Implementation of Modern Technologies in Avionic Systems".

ABSTRACT The article is mainly devoted to the analysis of the transient process during the phase change of the intra-impulse modulated signal of the system, which is composed of a pair of piezoelectric ceramic transducers. In the introductory part, this article is focused on the most accurate determination of the parameters of electrical equivalent circuit of piezoelectric ceramic transducers commonly available on the market of electrical components and less economically demanding. Based on the determination of these parameters, a system consisting of the piezoelectric ceramic transducer, transmitter - environment - piezoelectric ceramic transducer, receiver is then assembled and represented by transfer function. This system is subjected to simulation. An intra-impulse modulated signal with phase modulation is connected to the system input. The response to this signal is subsequently analyzed and compared with the real response of a real system. The goal is therefore to verify the suitability of the simulation model and, on the basis of this analysis, to determine the possibility of using specific piezoelectric ceramic transducers for application of intra-impulse modulated signal. As a method of verification, main parameter analysis of a cross-correlation function was selected. Based on this analysis it was found that this method is relevant for this purpose.

INDEX TERMS Cross-correlation function, impedance analysis, intra-impulse modulation, optimization, piezoelectric ceramic transducer, simulation.

I. INTRODUCTION

Significant part of the piezoelectric ceramic transducers is the piezo-ceramic. Piezo-ceramic is used in various applications to convert electrical energy into mechanical energy and vice versa. Important advantage of piezo-ceramic contrary to piezo-crystal is that they can be shaped into almost any form. The most common forms, that are used, are: rings, discs, cylinders, rectangular plates and hemispherical bodies. Another implementation that uses piezo-ceramic are monolithic multilayer drivers. Piezoelectric properties are subsequently created by the effect of a strong electrostatic field. Piezoelectric ceramic transducers are used for converters, for sensors, for drivers and also for various special applications [1], [2]. This article is mainly devoted to ultrasonic sensors that are commonly available on the market and are not economically demanding. An example of such sensors is shown in fig. 1. They are sensors from the companies Murata and Multicomp Pro in the application for the propagation of acoustic waves in the air and in liquid and for the function of transmitter, receiver and transceiver.

The most common application in which these sensors are used is the measurement of a distance of an obstacle. The distance is evaluated here on the principle of determination of the time of arrival of the acoustic wave [3]. This principle can be implemented into transport or handling means to avoid the collisions with unwanted obstacles. Another option is the implementation to unmanned vehicles for maintaining a certain safe distance from an obstacle or maintaining a certain constant flight height above the terrain [4], [5], [6]. The principle of distance measurement using ultrasonic

technology can also be used to measure the level of a liquid. From this, it is possible to derive the amount of fuel in the specific fuel tank of the mean of transport [7].

For applications that require high demands in term of safety or possession protection, it is necessary that the distance is measured with high accuracy. One of the methods to make the distance measurement more accurate is the use of an intra-impulse modulation of the excitation signal of the piezoelectric ceramic transducer [8]. Amplitude, frequency and phase modulations are offered. For the actual application of a modulated signal to a specific piezoelectric ceramic transducer, it is necessary to determine the expected behavior of the system and then determine the suitability of the transducers for the given application. This article is mainly devoted to this issue.

FIGURE 1. Piezoelectric ceramic sensors [9].

The main aim and also the contribution of this article is primarily in the idea. A model of the complete transmitter-environment-receiver system is created here, which is represented by a transfer function. The derivation of the transfer function in such a configuration and from such a point of view has not been published yet. The responses of this system to intra-impulse phase-modulated different signals are performed in a simulation environment. Furthermore, the real responses of this system to the intra-impulse phase-modulated signals with specific piezoelectric ceramic transducers are also experimentally verified. The similarity of simulated and real responses is analyzed through the main parameters of the cross-correlation function. Main lobe width (HPBW) and sideband suppression level (PSLR) were determined as the main parameters of the cross-correlation function because they can quantitatively and unambiguously determine the similarity between two signals. A significant advantage is that they can be easily determined from the course of this function. Based on the analysis using the cross-correlation function, it is possible to conclude whether the system model is built correctly or with what limitations. If the procedure is correct, a model is therefore available that is significantly close to the real system. Therefore, it is then possible to use the assembled model, to determine the nature of the response to almost any signal only with the use of a simulation environment, and there is no need for a complete real workplace, which is the main benefit of the proposed algorithm. The only thing that is needed from a real measurement is to find out the impedance spectrum of specific piezoelectric ceramic transducers. All measurements, tests and analysis were performed on specific piezoelectric ceramic transducers commonly available on the market, which was also an important aim of the work. With the use of the presented algorithm is possible to get information - specific models, which cannot be obtained from the technical documentation provided by the manufacturer of these circuits.

II. ELECTRICAL EQUIVALENT CIRCUIT OF PIEZOELECTRIC CERAMIC TRANSDUCER

In ultrasonic sensor applications, a piezoelectric ceramic transducer is used as a transmitter as well as a receiver. Therefore, before developing a specific application, it is necessary to create electrical equivalent circuits for both the piezoelectric ceramic transducer transmitter and receiver. There are several approaches to create the circuit [10]. The most frequently used electrical equivalent circuit is a simplified unloaded Butterworth-Van-Dyke circuit. This circuit primarily represents a piezoelectric ceramic transducer from the point of view of the electrical domain. This article is focused on the electrical domain, thus excitation by an electrical signal and reception of an electrical signal for further processing [11]. Schemes of these electrical equivalent circuits of the piezoelectric ceramic transducer - transmitter and receiver are shown in fig. 2.

The electrical scheme of both the transmitter and the receiver consists of the equivalent of a mechanical oscillator and the electrical part of the transducer. The mechanical oscillator is represented by a series combination of resistor R_S, coil L_S and capacitor C_S. The resistor R_S represents mechanical damping, the coil L_S effective mass and the capacitor C_S mechanical compliance. The electrical element of the transducer consists of a blocking capacitor C_P [11]. In the case of the transmitter, electrical energy is converted into mechanical energy. An input electrical signal is applied to the entire circuit, which is characterized by the voltage V_{1T}. The acoustic energy that subsequently spreads into the space corresponds to the losses on the R_S resistor. The output signal from the transmitter is then the force in this case presented by the voltage V_{2T}. On the receiver side, mechanical energy is converted back into electrical energy. The power supply for the receiver circuit here is the voltage source in the branch of the electrical equivalent circuit of the mechanical oscillator, represented by the voltage V_{2R}. The output electrical signal is the voltage V_{3R}.

In order to create the model of the complete system, it was necessary to determine the individual parameters of the electrical equivalent circuit of the piezoelectric ceramic transducer. These parameters are therefore R_S, L_S, C_S and C_P. These parameters were determined from the impedance characteristics of specific piezoelectric ceramic transducers commonly available on the market. Transducers listed below are also not very economical demanding.

Therefore, transducers marked MCUSD16A40S12R0 from the company Multicomp Pro were used. These transducers

allow to work as a transmitter as well as a receiver. First, the impedance characteristics were measured - the dependence of the impedance magnitude and the impedance angle on the frequency using a circuit analyzer. As it is stated in the technical documentation [12] that the given transducer works with resonant frequency of 40 kHz and the directivity of 50°, the mentioned characteristics were measured around that frequency. The sound pressure level of the transducers is at least 110 dB (10 V/30 cm). The frequency range was chosen to be 38 – 42 kHz. The test signal was harmonic with the amplitude of 1 V. The temperature at the time of measurement was 22 °C. Due to the fact that the plan was to subsequently use these converters in complete system, transmitter – environment - receiver, the mentioned characteristics were measured for two transducers, one for each purpose. The measured characteristics are in fig. 3 and fig. 4.

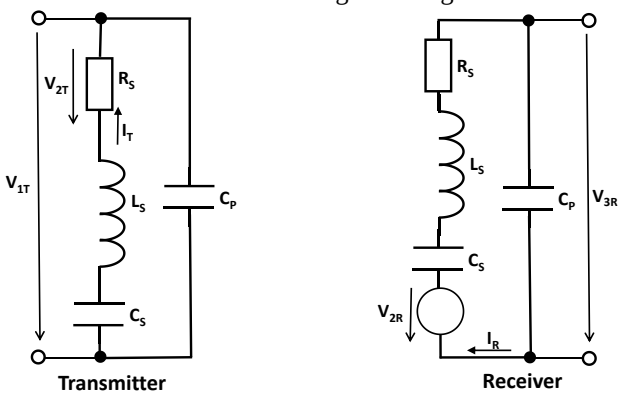

FIGURE 2. Electrical equivalent circuits of the piezoelectric ceramic transducer in the function of transmitter and receiver.

As is possible to see from the pictures, although they are identical types of transducers, they show different characteristics. Other transducers will have different characteristics too. From these measured characteristics, the parameters of the electrical equivalent circuit of piezoelectric ceramic transducers were calculated and subsequently optimized according to the algorithm, which was based on the methods presented in [13], [14], [15]. The parameters were R_S, L_S, C_S and C_P. The MATLAB® development environment was used for calculations, optimization and rendering of the characteristics. For optimization to specify the required parameters, a function, which is implemented directly in the basic version of the MATLAB® development environment was used. It is the function fminsearch(fun,x0,options) [16]. The individual arguments of the function mean: fun – criterion function for which the minimum is sought, x0 – initial conditions of the iteration and options – optimization settings. Therefore, the minimum optimization method is used here. The optimization algorithm uses the fact that it gradually changes the parameters of the components of the electrical equivalent circuit of the piezoelectric ceramic transducer (R_S, L_S, C_S and C_P) until the minimum possible difference in the absolute value of the difference in the magnitude of the impedance calculated from these parameters and measured by the impedance spectroscope is reached. The criterion function is defined by this way.

The following figures and tables show the optimization results. It was found that the results of the optimization differ depending on the frequency range in which the optimization is performed and whether it is performed in the entire measured range or only in a narrow area of the series or parallel resonant frequency of the transducer. Series resonance on the characteristics is represented by a local minimum and parallel resonance by a local maximum, which are therefore significant points of the characteristics [17], [18], [19]. It appears that it will be different for different transducers (characteristics). At the measured transducers, for the transmitter, the best results were achieved when optimizing for the entire measured frequency range, while for the receiver, it was for the optimization near the series resonance frequency.

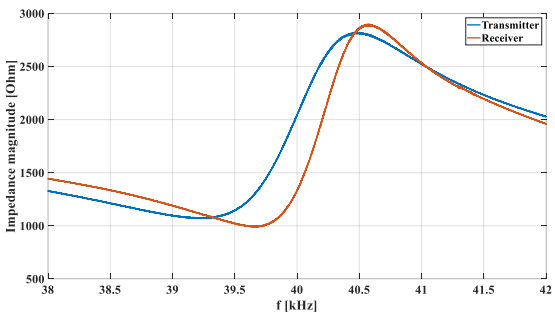

FIGURE 3. The dependence of impedance magnitude on frequency.

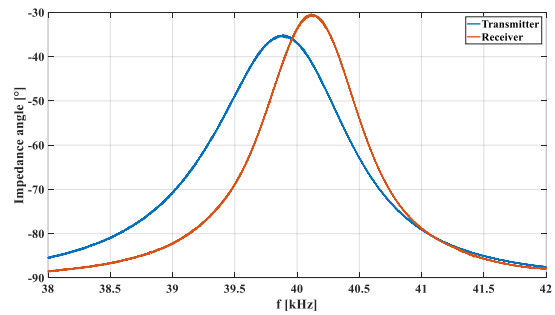

FIGURE 4. The dependence of impedance angle on frequency.

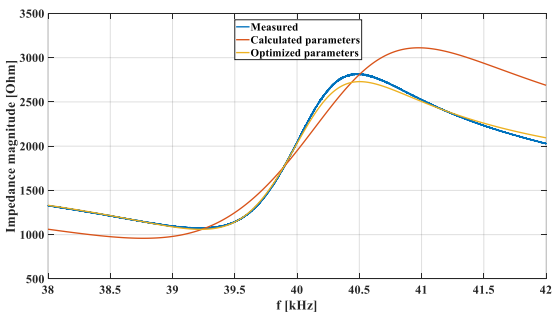

FIGURE 5. The dependence of impedance magnitude on frequency for transmitter.

Measured, calculated and optimized characteristics for transmitter show fig. 5 and fig. 6.

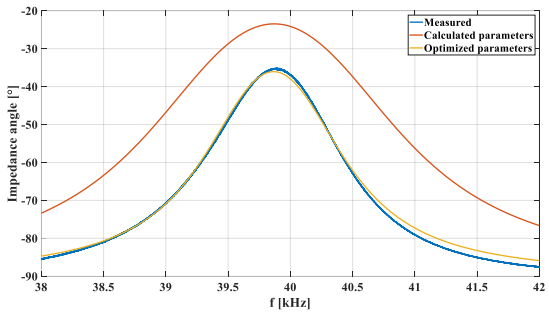

FIGURE 6. The dependence of impedance angle on frequency for transmitter.

Table I shows the values of the calculated and optimized parameters of the electrical equivalent circuit of the piezoelectric ceramic transducer - transmitter.

TABLE I
THE VALUES OF THE CALCULATED AND OPTIMIZED PARAMETERS OF THE ELECTRICAL EQUIVALENT CIRCUIT OF THE PIEZOELECTRIC CERAMIC TRANSDUCER – TRANSMITTER

	R_{ST} [Ω]	L_{ST} [H]	C_{ST} [F]	C_{PT} [F]
Calculated	1336	0.1111	$1.4792 \cdot 10^{-10}$	$2.2757 \cdot 10^{-9}$
Optimized	1683	0.2291	$7.0594 \cdot 10^{-11}$	$2.3306 \cdot 10^{-9}$

Table I shows that the values of the components of the equivalent circuit of the piezoelectric ceramic transducer - transmitter, which were found by calculation, are significantly different from the optimized values, except for C_P. Therefore, optimization had to be done. This is very clearly shown by the characteristics depicted above, which are also significantly different. Series and parallel resonant frequencies are different. Impedance values at these frequencies also differ significantly. The dependence of the impedance angle on the frequency is shifted to higher values. These characteristics and values of the components of the electrical equivalent circuit of a given transducer essentially represent a different equivalent circuit. To evaluate the accuracy of the calculation and optimization, the relative errors of significant characteristic points were determined. Table II represents these relative errors.

TABLE II.
RELATIVE ERRORS OF SIGNIFICANT CHARACTERISTIC POINTS OF ELECTRICAL EQUIVALENT CIRCUIT OF PIEZOELECTRIC CERAMIC TRANSDUCER – TRANSMITTER

	δ_{fs} [%]	δ_{fp} [%]	δ_{fu} [%]	δZ_{fs} [%]	δZ_{fp} [%]	δ_u [%]
Calc.	1.2422	1.1526	0.0409	10.2991	10.3186	33.1128
Opt.	0.0660	0.0151	0.0529	0.8847	3.2400	2.8142

Errors values are in the following order: δ_{fs} – relative error of the series resonant frequency, δ_{fp} – relative error of the parallel resonant frequency, δ_{fu} – relative error of the frequency at maximal angle in the resonant area, δZ_{fs} – relative error of the impedance magnitude at series resonance, δZ_{fp} – relative error of the impedance magnitude at parallel resonance, δ_u – relative error of the maximal impedance angle in the resonance area.

From the relative error values, it can be seen that the optimization algorithm significantly precised the above-mentioned characteristics.

The same was done for the piezoelectric ceramic transducer - receiver. The measured, calculated and optimized characteristics for the receiver are shown in fig. 7 and fig. 8. The values of the optimized parameters of the electrical equivalent circuit of the piezoelectric ceramic transducer - receiver are shown in table III.

TABLE III
THE VALUES OF THE CALCULATED AND OPTIMIZED PARAMETERS OF THE ELECTRICAL EQUIVALENT CIRCUIT OF THE PIEZOELECTRIC CERAMIC TRANSDUCER – RECEIVER

	R_{SR} [Ω]	L_{SR} [H]	C_{SR} [F]	C_{PR} [F]
Calculated	1205	0.1504	$1.0714 \cdot 10^{-10}$	$2.3278 \cdot 10^{-9}$
Optimized	1488	0.2805	$5.6755 \cdot 10^{-11}$	$2.3277 \cdot 10^{-9}$

Table III and characteristics in fig. 7 and fig. 8 again show significant difference in the parameters of the equivalent circuit for the receiver as well.

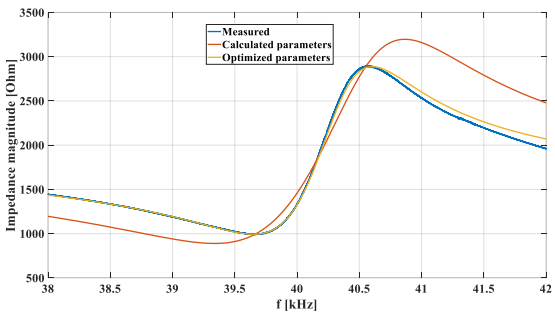

FIGURE 7. The dependence of impedance magnitude on frequency for receiver.

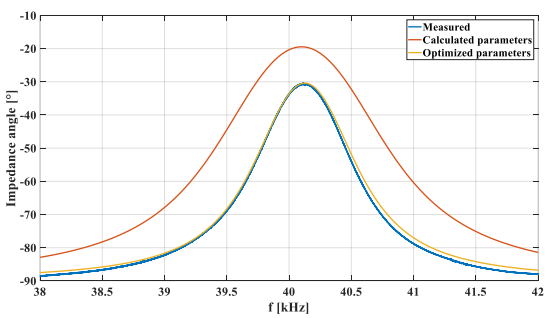

FIGURE 8. The dependence of impedance angle on frequency for receiver.

To evaluate the accuracy of the calculation and optimization, the relative errors of significant characteristic points were determined again. Table IV represents these relative errors.

TABLE IV
RELATIVE ERRORS OF THE SIGNIFICANT CHARACTERISTIC POINTS OF THE ELECTRICAL EQUIVALENT CIRCUIT OF THE PIEZOELECTRIC CERAMIC TRANSDUCER – RECEIVER

	δ_{fs} [%]	δ_{fp} [%]	δ_{fu} [%]	δZ_{fs} [%]	δZ_{fp} [%]	δ_u [%]
Calc.	0.8024	0.7604	0.0349	9.9450	10.2673	35.8981
Opt.	0.0151	0.1161	0.0292	0.5966	0.3953	0.1498

From the relative error values, it can again be seen that the optimization algorithm significantly increased the accuracy of the important points of the characteristics of the piezoelectric ceramic transducer. The values of the relative errors mostly reach tenths and hundredths of percent, only in two cases there were units of percent. The maximum relative error of the optimization algorithm was 3.2400%. In contrast, the maximum relative error in the case of determining the parameters of the equivalent circuit by calculation was 35.8981%, which is a relatively high value.

III. TRANSFER FUNCTION OF THE SYSTEM

Based on the optimized parameters of the electrical equivalent circuit of the piezoelectric ceramic transducer - transmitter and receiver, it was possible to assemble the transfer function of the system for analyzing the response to various signals with intra-impulse phase modulation. Fig. 9 characterizes the illustrative scheme of the mentioned system.

FIGURE 9. Illustrative scheme of the system.

The system is composed of three important blocks. One of the blocks is the transfer function, which represents here the piezoelectric ceramic transducer - transmitter. The following is the block that represents the environment through which the acoustic wave propagates, and total amplification of the system can also be integrated here. The last block is again the transfer function, which represents here the piezoelectric ceramic transducer - receiver. A signal enters into the system, which in this case will represent intra-impulse modulated waveforms. A signal of the response emerges from the system and is displayed and subjected to further analysis.

To compile the transfer function of the entire system, it is necessary to derive these functions for individual blocks. The derivation of the transfer function of the transmitter is based on the diagram in fig. 2. The Laplace transform is also used to derive this function. For derivation of the transfer function of the transmitter $G_T(s)$, the following formula is applied.

$$G_T(s) = \frac{V_{2T}(s)}{V_{1T}(s)}, \tag{1}$$

where $V_{2T}(s)$ is output voltage in Laplace transform, $V_{1T}(s)$ is input voltage in Laplace transform and s is Laplace operator.

For the current $I_T(s)$ flowing through the electrical equivalent circuit of the mechanical oscillator following formula is applied:

$$I_T(s) = \frac{V_{1T}(s)}{R_{ST} + L_{ST}\cdot s + \frac{1}{C_{ST}\cdot s}}. \tag{2}$$

For voltage $V_{2T}(s)$ is then applied:

$$V_{2T}(s) = \frac{R_{ST}\cdot V_{1T}(s)}{R_{ST} + L_{ST}\cdot s + \frac{1}{C_{ST}\cdot s}}. \tag{3}$$

After the final adjustments of this formula, the resulting transfer function of the transmitter into the simulation model is obtained.

$$G_T(s) = \frac{s}{\frac{L_{ST}}{R_{ST}}s^2 + s + \frac{1}{R_{ST}\cdot C_{ST}}}. \tag{4}$$

Hereby, all the important parameters and characteristics for the piezoelectric ceramic transducer - transmitter are determined.

Transfer function of the environment $G_E(s)$, through which an acoustic wave propagates is represented here by equation:

$$G_E(s) = G_S(s)\cdot e^{-\tau\cdot s}, \tag{5}$$

where $G_S(s)$ is the system gain, τ is the system delay – it mainly corresponds to the time of arrival of the acoustic wave.

Additional amplification can be integrated into the G_S, for example, the necessary amplification of signals to the required level, amplification due to the acoustic wave interference caused by inhomogeneities in the environment or reflection from the transducers to each other or from an obstacle, and amplification caused by the absorption of the acoustic wave by an obstacle.

To determine the transfer function of the receiver, the scheme in fig. 2, the Laplace transform and a similar procedure as for the transmitter were also used. For the transfer function $G_R(s)$, the following equation is defined:

$$G_R(s) = \frac{V_{3R}(s)}{V_{2R}(s)}, \tag{6}$$

where $V_{3R}(s)$ is output voltage and $V_{2R}(s)$ is input voltage.

For the current $I_R(s)$, which in this case flows through the electrical equivalent circuit of the mechanical oscillator and the capacitor C_{PR}, the following equation is applied:

$$I_R(s) = \frac{V_{2R}(s)}{R_{SR} + L_{SR}\cdot s + \frac{1}{C_{SR}\cdot s} + \frac{1}{C_{PR}\cdot s}}. \tag{7}$$

For voltage $V_{3R}(s)$ is then applied:

$$V_{3R}(s) = \frac{V_{2R}(s)}{C_{PR}\cdot s\cdot(R_{SR} + L_{SR}\cdot s + \frac{1}{C_{SR}\cdot s} + \frac{1}{C_{PR}\cdot s})}. \tag{8}$$

After the final adjustments of this expression, the resulting transfer function of the receiver to the simulation model is obtained.

$$G_R(s) = \frac{1}{L_{SR}\cdot C_{PR}\cdot s^2 + C_{PR}\cdot R_{SR}\cdot s + \frac{C_{PR}}{C_{SR}} + 1}. \quad (9)$$

This achieves all the necessary parameters and characteristics of the piezoelectric ceramic transducer - receiver. The resulting transfer function of the entire system transmitter – environment – receiver $G_{WS}(s)$, which is then further worked with in the MATLAB® development environment, is then defined by the equation:

$$G_{Ws}(s) = \frac{s}{\frac{L_{ST}}{R_{ST}}\cdot s^2 + s + \frac{1}{R_{ST}\cdot C_{ST}}} \cdot G_S(s) \cdot e^{-\tau\cdot s} \cdot \frac{1}{L_{SR}\cdot C_{PR}\cdot s^2 + C_{PR}\cdot R_{SR}\cdot s + \frac{C_{PR}}{C_{SR}} + 1}. \quad (10)$$

Fig. 10 illustrates the transfer function frequency characteristics of the complete system to be analyzed. The optimized parameters of the equivalent electrical circuit of the piezoelectric ceramic transducer transmitter and receiver from the previous section are used here. The frequency characteristics are depicted in the same range as the impedance spectra, thus from 38 kHz to 42 kHz. The upper curve is the magnitude frequency characteristic and the lower curve is the phase frequency characteristic. The resonant frequency of the entire system is 40.2 kHz. The bandwidth is 1.1 kHz. The magnitude of the transfer function at the frequency of 38 kHz is -23.1 dB and at the frequency of 42 kHz is -23.4 dB. The phase of the transfer function varies from 60.2° to -241.0° in the mentioned frequency range. At the resonant frequency, the phase is -115°.

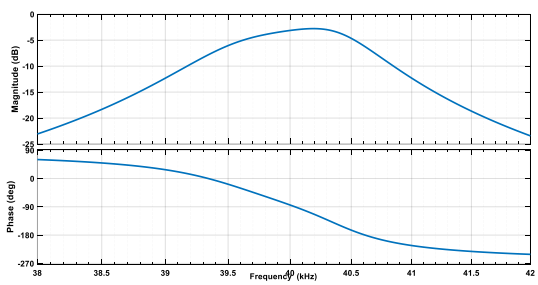

FIGURE 10. **Frequency characteristics of the entire system.**

IV. EXPERIMENTAL ANALYSIS

To obtain responses from a real system and to perform subsequent transmitting part analysis, of the above-mentioned piezoelectric ceramic transducer a test platform has been assembled representing the whole transmission line, including the environment and the receiving part with the transducer, see fig. 11. This picture essentially corresponds to fig. 9 and the derivation of the transfer functions from the previous section. Here, the Transmitter is represented by equation (4), the Receiver is represented by equation (9). The environment, which is defined by relation (5), here represents the space of propagation of the acoustic wave from the Transmitter to the wall, its reflection from the wall and again propagation to the Receiver. Amplification at the transmitter and receiver is also included in the transfer function of the environment. Only electrical signals are used here. So, there are the signals that excite the Transmitter and the following signals that come out of the Receiver. The exact nature of an acoustic wave propagation in this environment is not included in the model, because the already mentioned electrical signals are needed for further analysis.

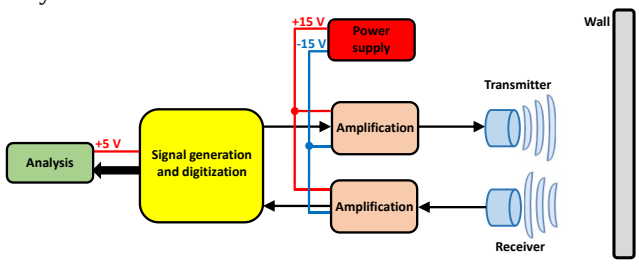

FIGURE 11. **Test platform used to obtain realistic system responses.**

The aforementioned piezoelectric ceramic transducers in a transmitter and receiver configuration were placed 0.5 m from the wall. A Red Pitaya device [20] was used to generate the required excitation signals for the transmitter and to digitize the received signals as well. Digital analogue converter resolution for output as well as for input signal was 14 bit. The excitation signal for the piezoelectric ceramic transducer - transmitter was amplified so that the generated amplitude was constant with the value of 1 V. Additional amplification was also performed in the receiving section to get the amplitude of the received signal close to 1 V as well. The response of the whole transmission line to the input signals sent by the Red Pitaya device was recorded via Red Pitaya to a laptop computer where the transmitted and received signals were displayed and the following analysis was performed. The laptop served as the power system for the Red Pitaya device and a laboratory power supply was used as a power supply for the amplifiers.

Two-state and four-state phase-modulated signals – Gold and Kasami codes (sequences) [21] were used as excitation signals for the piezoelectric ceramic transmitter. Gold sequences are most often used in telecommunications and satellite navigation [22]. Kasami sequences are very often used in code division multiple access systems [23]. These codes stand out by having a very low cross-correlation within the generated set of codes [22], [23], [24], [25], [26], [27], [28]. These binary code sequences were thus sequentially generated and fed to the piezoelectric ceramic transmitter and the respective responses from the piezoelectric ceramic receiver were digitized and further analyzed. The Gold

sequences were generated by 5th order polynomials. Sequences from the so-called Minimum Length Sequences (MLS) group were selected. A set of Gold codes for testing and analysis was created using the preferred pair [5, 4, 3, 2] and [5, 2]. The set had 33 codes of 31 bits in length. A table of these codes was therefore created, which is in the Supplementary materials. Small Kasami sequences 6th order polynomials were used. Sequences from the MLS group were also selected. A set of Kasami codes for testing and analysis was created using the preferred pair [6, 1]. The set had 8 codes with a length of 63 bits. A table of these codes was created again, which is in the Supplementary materials. A detailed description of the generation of individual code sequences is described in the reference [29]. Based on this reference, generators for Gold and small Kasami sequences were created in the MATLAB® development environment, which created sequence tables of these codes. Properly working generators with comments of the appropriate codes that are used in the research in this article (gold_5.m, kasami_pokus.m) were added to the Supplementary materials too. Fig. 12 represents an example of the real and simulated response of the system to the excitation signal where a two-state Gold sequence was used.

The excitation signal used for the piezoelectric ceramic transmitter is drawn in blue. The frequency of the signal is 40 kHz. Changes in the signal phase are visible as light vertical lines on the waveform. The orange color represents the simulated received signal and the red color represents the signal measured from the real transducer. The delay of the returning signal corresponding to the time of flight of the acoustic wave has been removed on the purpose so that the response to the change in the phase of the input signal can be more clearly seen. By comparing the simulated and the measured signal, it is possible to conclude that the two signals are remarkably similar. A similar response to a 180° phase change is evident here. To ascertain the similarity of these signals more detailed analysis was needed, therefore a cross-correlation function was applied to determine the relevance of the system model.

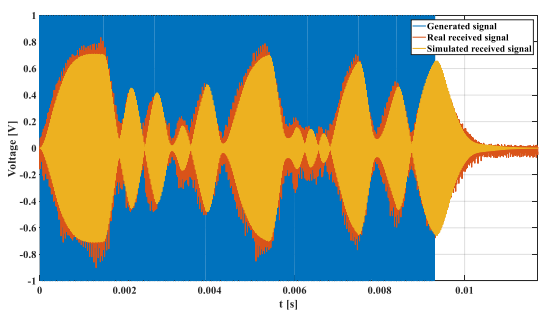

FIGURE 12. **Real and simulated response to the excitation signal.**

The cross-correlation function between the input and the simulated signal and between the input and the real measured output signal from the transducer was calculated for each type of intra-impulse modulation. Furthermore, the cross-correlation function between individual code orders was calculated again for each type of intra-impulse modulation. Important correlation function parameters such as main lobe width (HPBW) and sideband suppression level (PSLR) were evaluated. Fig. 13 shows an example of such a correlation function with the analysis parameters marked.

Fig. 14 shows the width of the main lobe of the correlation function and fig. 15 shows the sideband suppression level of the correlation function for a real received signal and a simulated received signal and individual code sequences. Once again a two-state Gold sequence is depicted. A bar graph was chosen for visual clarity. The above-mentioned parameters of the correlation function for the measured signal are represented by blue bars and for the simulated signal by red bars.

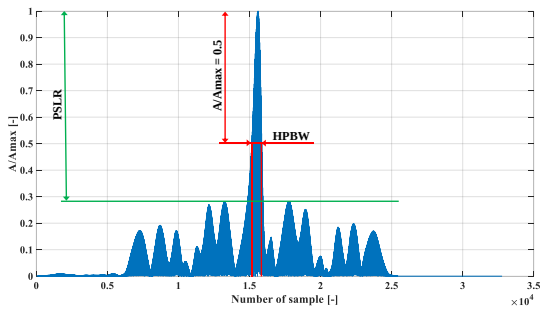

FIGURE 13. **An illustrative example of the correlation function and its parameters.**

Fig. 14 shows that there is a relatively high difference in the width of the main lobe of the correlation function for code order 5. The next high difference is for code order 3. A very small difference in these parameters is for the order of code 18. Other code orders show mostly little difference in these parameters. Important statistical indicators were determined to quantify the difference in these parameters. The minimum difference in the widths of the main lobe of the correlation function of the measured and simulated signal is 13 samples, the maximum is 818 samples, and the mean value of this parameter is 159 samples. The time interval between two samples is 1.024 μs, which in the case of the mean value of this parameter corresponds to 162.816 μs. Fig. 15, shows that the most significant difference in the sideband suppression levels of the correlation function is for code order 4. The minimum difference, where these parameters appear to be almost identical, is for code order 8. For the other code orders, the differences in these parameters are mostly negligible.

Repeatedly, important statistical parameters were determined to quantify the difference in these parameters. The minimum difference in sideband suppression levels of the correlation function of the measured and simulated signal

is 0.032 dB, the maximum is 3.775 dB, and the mean value of this parameter is 0.960 dB.

For other sequences such as four-state Gold, two-state, and four-state Kasami, the analysis results are presented in Table V and Table VI. Table V contains important statistical indicators for the difference in the widths of the main lobe of the correlation function of the measured and simulated signal. From the statistical indicators, it can be concluded that the measured and simulated signals are the most similar in the case of the four-state Kasami sequence. The biggest differences in the analyzed parameters are in the case of the two-state Gold sequence.

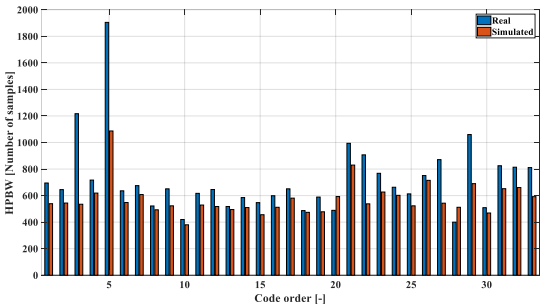

FIGURE 14. **Width of the main lobe of the correlation function for a two-state Gold sequence.**

TABLE V
SIGNIFICANT STATISTICAL PARAMETERS FOR THE WIDTHS DIFFERENCE IN THE MAIN LOBE OF THE CORRELATION FUNCTION

	Gold BPSK	Gold QPSK	Kasami BPSK	Kasami QPSK
Difference minimum [Number of samples]	13	5	1	2
Difference maximum [Number of samples]	818	506	250	153
Difference mean value [Number of samples]	159	132	119	70

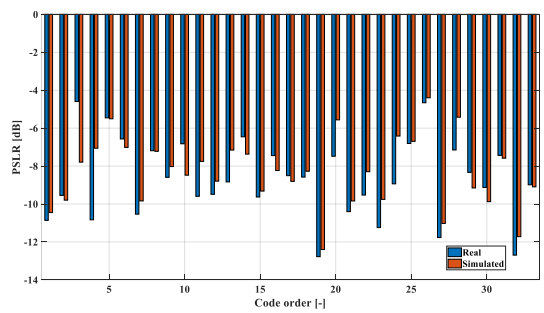

FIGURE 15. **Sideband suppression level for a two-state Gold sequence.**

Table VI contains important statistical indicators for the sideband suppression levels difference in the correlation function of the measured and simulated signal. This time, it is not possible to decide which sequence according to all the analyzed parameters of these signals is closest to each other, but considering the maximum and mean values, a four-state Kasami sequence can be chosen again. The biggest difference, based on the mean value, is in the two-state Kasami sequence.

Afterward, only one parameter of the cross-correlation functions between the individual code orders was analyzed again for the measured and simulated received signal, namely the suppression of the sideband levels. Fig. 16 illustrates the differences in this parameter of both signals for a two-state Gold sequence. For the sake of clarity, a bar graph was chosen again and only the difference in the suppression levels of the sidebands of these two signals are presented. This is three-dimensional graph, where mentioned parameter of cross-correlation function is at vertical axis and code orders are at horizontal axes. Such an arrangement is in order to see how the difference of the relevant parameter of the cross-correlation function develops for all possible mutual combinations of individual code orders. So the bar chart for Gold codes contains 1089 columns and the bar chart for Kasami codes contains 64 columns. Fig. 17, 18, 19 represent bar charts for the rest of the codes tested and analyzed.

TABLE VI
SIGNIFICANT STATISTICAL PARAMETERS FOR THE SIDEBAND SUPPRESSION LEVELS DIFFERENCE IN THE CORRELATION FUNCTION

	Gold BPSK	Gold QPSK	Kasami BPSK	Kasami QPSK
Difference minimum [dB]	0.032	0.012	0.003	0.041
Difference maximum [dB]	3.775	4.596	3.203	1.229
Difference mean value [dB]	0.960	0.956	1.111	0.596

To tell the difference between the measured and simulated signal in this parameter, it is again necessary to establish important statistical indicators. The minimum difference in the sideband suppression level of the cross-correlation function of the real and simulated received signal is 0.0004 dB, the maximum is 3.5813 dB, and the average value of this parameter is 0.9480 dB. For the other sequences, the results of the analysis are given in Table VII.

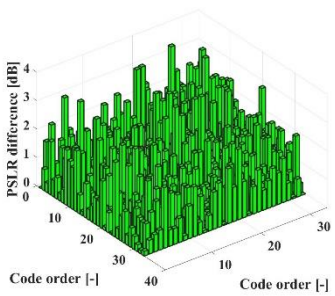

FIGURE 16. **Difference in sideband suppression levels of the cross-correlation function for a two-state Gold sequence.**

TABLE VII
SIGNIFICANT STATISTICAL PARAMETERS FOR THE DIFFERENCE IN SIDEBAND SUPPRESSION LEVELS OF THE CROSS-CORRELATION FUNCTION BETWEEN INDIVIDUAL CODE ORDERS

	Gold BPSK	Gold QPSK	Kasami BPSK	Kasami QPSK
Difference minimum [dB]	0.0004	0.0003	0.0160	0.0200
Difference maximum [dB]	3.5813	3.3006	5.0926	1.6161
Difference mean value [dB]	0.9480	0.7552	1.5967	0.7340

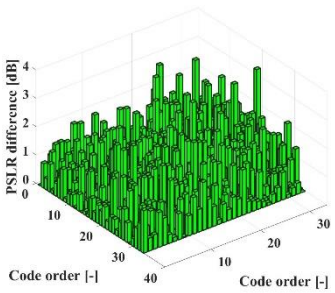

FIGURE 17. Difference in sideband suppression levels of the cross-correlation function for a four-state Gold sequence.

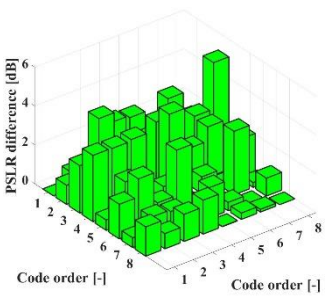

FIGURE 18. Difference in sideband suppression levels of the cross-correlation function for a two-state Kasami sequence.

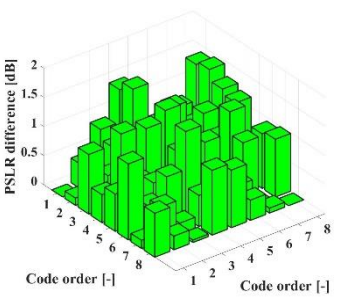

FIGURE 19. Difference in sideband suppression levels of the cross-correlation function for a four-state Kasami sequence.

From the point of view of the mean value of the analyzed parameter, it can be determined that the smallest difference between the real and simulated received signal is again in the case of the four-state Kasami sequence. The biggest difference is in the two-state Kasami sequence.

V. CONCLUSION

This article was primarily aimed at the verification of behavior in the transmitter – environment - receiver system model in response to phase-modulated excitation signals. Narrow-band ultrasonic piezoelectric ceramic transducers, commonly available on the electronic component market and economically undemanding, were used as transmitter and receiver. The ambition was to determine suitability for the above-mentioned applications.

Firstly, electrical equivalent circuits were defined and optimized for two specific transducers that worked as transmitter and receiver. For further analysis, only electrical signals were used, thus excitation signals for the piezoelectric ceramic transducer - transmitter and signals from the receiver, therefore the most commonly used electrical equivalent circuit Butterworth-Van-Dyke was chosen. The nature of acoustic wave propagation in space was not included in the model. Although they were supposed to be identical converters according to the manufacturer, by measuring and subsequently determining the parameters of the electrical equivalent circuits, it was found that they were slightly different, as shown by the measurement data.

Secondly, the transfer functions of the entire transmitter – environment – receiver system were derived. The transfer functions were mainly focused on the transmitter and receiver, therefore the environment model expressed by the transfer function was to some degree simplified here. Environment model was simplifier according the statement above. The derivation of the complete transfer function in such a configuration of piezoelectric ceramic transducers has not been published in the literature yet.

This was subsequently followed by the necessary simulations and comparison with real measured signals and their analysis was performed. Two-state and four-state Gold and Kasami sequences were implemented as input signals. Cross-correlation functions and their significant parameters, such as main lobe width and sideband suppression level, were used to evaluate the model. Cross-correlation functions between the input signal and the real received signal as well as between the input signal and the simulated received signal were calculated for all sequences. Furthermore, calculations of cross-correlation functions were performed for all combinations of code order for real and simulated received signals, as well as for all sequences. An important parameter for the analysis of the similarity of individual signals was the difference in the mentioned parameters of the cross-correlation function. Important statistical indicators were calculated for this parameter.

All the waveforms as well as all the analyses of the parameters of the cross-correlation function, and all the measurements and simulations performed showed a significant similarity. The four-state Kasami sequence

showed the best agreement between the real and the simulated signal. The worst agreement of these signals based on the parameters of the correlation function cannot be determined.

Based on the above analyses, it can be assumed that the derived system model is relevant for determining the suitability of a given piezoelectric ceramic transducer for the required applications. The reaction to a change in the phase of the input signal by 180° is important here, as it represents a significant change for a mechanical system. The derived system model responds to this phase change correctly and with a high degree of similarity to the real system, as indicated by the analysis presented in this article. Therefore, it is possible to say in general that with the help of the derived model it is practicable to determine the expected character of the transition process during the change of the phase of the excitation signal for specific piezoelectric ceramic transducers and thus determine the suitability for phase modulated signals. Therefore, it is not necessary to build a complete real system, but the analysis can be carried out with the help of a simulation environment. The only thing that needs to be measured realistically are the impedance spectra of specific piezoelectric ceramic transducers. On the basis of a very accurate derivation of the parameters of the electrical equivalent circuit of the piezoelectric ceramic transducers, it is possible to significantly approach the real system, which was shown by experimental measurements and its analysis. The contribution of the article is therefore mainly in the idea presented and in the complete proposed algorithm. Another important benefit is that with the use of this algorithm, very accurate models of specific piezoelectric ceramic transducers available on the market can be obtained, which cannot be ascertained from the manufacturer's technical documentation. However, the disadvantage of the presented algorithm is the simplification of the environment model. A more sophisticated environment model will contribute to the refinement of the complete system model, which will bring it even closer to the real system.

ACKNOWLEDGMENT

The work presented in this article was supported by the Czech Republic Ministry of Defence – University of Defence Development Program – "Conduction of Operations in Airspace", the Czech Republic Ministry of Education, Youth and Sports – University of Defence student research program "Modern Methods of Generation, Direction Control and Signal Processing" and the Czech Republic Ministry of Education, Youth and Sports – University of Defence student research program "Implementation of Modern Technologies in Avionic Systems".

REFERENCES

[1] M. Prokic, "Piezoelectric Transducers Modeling and Characterization", MPI, Switzerland, 2004.
[2] H. Liqing, F. Liwen, R. Xiaodan, Z. Shuguang, W. Sanhong, X. Zhuo, Y. Yongke, "High-temperature piezoelectric ultrasonic transducer based on BiScO3-PbTio3 ceramics", Sensors and actuators a-physical, vol. 362, pp. 1-10, 2023, doi: 10.1016/j.sna.2023.114657.
[3] P. Janů, R. Šrámek, "Intelligent Distance Measuring Module Using Ultrasonic Piezoelectric Ceramic Transducers", Przeglad Elektrotechniczny, vol. 96, no. 11, pp. 147-150, 2020, doi: 10.15199/48.2020.11.30.
[4] L. Xusheng, L. Jingjing, "An Adaptive Altitude Information Fusion Method for Autonomous Landing Processes of Small Unmanned Aerial Rotorcraft", Sensors, vol 12, no. 10, pp. 13212-13224, 2012, doi: 10.3390/s121013212.
[5] M. Błachuta, R. Czyba, W. Janush, G. Szafrański, "Data Fusion Algorithm for the Altitude and Vertical Speed Estimation of the VTOL Platform", Journal of Intelligent & Robotic Systems, vol 74, no. 1-2, pp. 413-420, 2014, doi: 10.1007/s10846-013-9917-4.
[6] N. Shijith, M. M. Dharmana, "Sonar Based Terrain Estimation & Automatic Landing of Swarm Quadrotors", in Proc International Conference on Circuits, Power and Computing technologies (ICCPCT), April 2017, pp. 1-4, doi: 10.1109/ICCPCT.2017.8074216.
[7] A. Sasidharan, "IHS Jane's Flight Avionics", IHS, 2016-2017.
[8] P. Dycka, P. Janu, J. Bajer, R. Bystricky, "Phase-Coded Modulation-Based Time-of-Flight Measurement Improvement for Piezoelectric Ceramic Transducers", IEEE Transactions on Ultrasonics, Ferroelectrics and Frequency Control, vol. 68, no. 4, pp. 1362-1369, 2021, doi: 10.1109/TUFFC.2020.3029329.
[9] „Ultrasonic Sensors." FARNELL. Accessed: Oct. 26, 2023. [Online]. Available: https://cz.farnell.com.
[10] A. A. Vives, "Piezoelectric Transducers and Applications", Springer, Germany, 2004.
[11] P. Janů, J. Bajer, P. Dyčka, R. Bystřický, "Precise Experimental Determination of Electrical Equivalent Circuit Parameters for Ultrasonic Piezoelectric Ceramic Transducers from Their Measured Characteristics", Ultrasonics, vol. 112, pp. 1-5, 2021, doi: 10.1016/j.ultras.2020.106341.
[12] "MULTICOMP PRO MCUSD16A40S12R0." Element 14. Accessed: Oct. 26, 2023. [Online]. Available: https://my.element14.com/multicomp/mcusd16a40s12ro/transceiver-40khz-16mm-metal/dp/2362677.
[13] A. Bybi, N. E. Atlas, H. Drissi, M. Garoum, A-C. Hladky-Hennion, "One-Dimensional Electromechanical Equivalent Circuit for Piezoelectric Array Elements", in Proc. International Conference on Electrical and Information Technologies (ICEIT 2017), 2017, pp. 1-5, doi: 10.1109/EITech.2017.8255214.
[14] R. Queirós, P. S. Girão, A. C. Serra. "Single-Mode Piezoelectric Ultrasonic Transducer Equivalent Circuit Parameter Calculations and Optimization Using Experimental Data." IMEKO. Accessed: Oct. 26, 2023. [Online]. Available: https://www.imeko.org/publications/tc4-2005/IMEKO-TC4-2005-084.pdf.
[15] Y. Zhao, G. L. Barbruni, Z. Li, L. Zhao, X. Wang, K. Wang, Z. Jiang, S. Carrara, "A Front-End CMOS Interface Circuit with High Voltage Charge Pump and Oscillator for Capacitive Micromachined Ultrasonic Transducers", IEEE Transactions on Circuits and Systems II – Express Briefs, vol. 70, no. 5, pp. 1799-1803, 2023, doi: 10.1109/TCSII.2023.3261061.
[16] "Fminsearch." MathWorks. Accessed: Oct. 26, 2023. [Online]. Available: https://www.mathworks.com/help/matlab/ref/fminsearch.html.
[17] N. Péres, M. A. B. Andrade, F. Buiochi, J. C. Adamowski, "Identification of Elastic, Dielectric, and Piezoelectric Constants in Piezoceramic Disks", IEEE Transactions on Ultrasonics, Feroelectrics and Frequency Control, vol. 57, no. 12, pp. 2772-2783, 2010, doi: 10.1109/TUFFC.2010.1751.
[18] Z. Yaowen, H. Linsheng, H. Ying, Z. Jing, "Admittance signature of piezoceramic transducers bonded on different materials", Journal of Intelligent systems and Structures, vol. 34, no. 10, pp. 1136-1144, 2023, doi: 10.1177/1045389X221128579.
[19] Z. Jingchao, L. Chenhui, H. Hao, S. Jinhua, L. Yingwei, J. Guoqian, L. Xiaoli, "Optimization Design of Piezoelectric Ceramic Ultrasonic Transducer Based on ANSYS Simulation", in Proc. Cross Strait Radio Science and Wireless Technology Conference, 2022, pp. 1-3, doi: 10.1109/CSRSWTC56224.2022.10098363.

[20] "STEMLab 125-14 Starter Kit." redpitaya. Accessed: Oct. 26, 2023. [Online]. Available: https://redpitaya.com/product/stemlab-125-14/.
[21] F. Xiong, "Digital Modulation Techniques", Artech House, inc., 2000.
[22] J. K. Holmes, "Spread Spectrum Systems for GNSS and Wireless Communications", Artech House, inc., 2007.
[23] A. N. Akansu, R. Poluri, "Walsh-Like Nonlinear Phase Orthogonal Codes for Direct Sequence CDMA", IEEE Transactions on Signal Processing, vol. 55, no. 7, pp. 3800-3806, 2007, doi: 10.1109/TSP.2007.894229.
[24] K. Anjana, S. Abdulhayan, "Performance analysis of CDMA spreading codes for LTE/MIMO", Journal of Pharmaceutical Negative Results, vol. 13, no. 3, pp. 1051-1054, 2022, doi: 10.47750/pnr.2022.13.S03.163.
[25] L. Tao, J. Sun, G. Li, B. Zhu, "An Improved Navigation Pseudolite Signal Structure Based on the Kasami Sequences and the Pulsing Scheme", Chinese Journal of Electronics, vol. 31, no. 2, pp. 220-226, 2022, doi: 10.1049/cje.2020.00.403.

Přemysl Janů was born in 1982 in Šternberk, Czech Republic. He received M.Sc. degree in Special Equipment of Aircraft in 2006 and Ph.D. degree in Electrical Systems and Devices in 2011 from the University of Defence in Brno, Czech Republic.

He is currently Head of Group of Avionics and Aircraft Armament Systems at the Department of Aviation Technology, Faculty of Military Technology, University of Defence. Now, his research interests include COTS piezoelectric ceramic transducers – electrical equivalent definition and simulation of a response on an input signals, sensors technology, sensors signal processing and inertial navigation systems.

Pavel Dyčka was born in Boskovice, Czech Republic in 1991. He received the B.Sc., M.Sc. and Ph.D. degrees in Avionic systems from the University of Defence in Brno in 2013, 2015 and 2021 respectively.

He is currently working at 22nd base of the helicopter air force, Náměšt nad Oslavou in the engineering aviation service. In recent years, his research interests have included ultrasonic distance measurement using COTS transducers and sensor fusion.

Josef Bajer received the B.Sc. degree in Electrical and Special Aircraft Equipment from the University of Defence in Brno (UDB), Czech Republic, in 2005, and the M.Sc. degree in Avionic Systems in 2008. The Ph.D. degree in Electronic Systems and Equipment he received from UDB in 2011.

He is currently Head of the Department of Aviation Technology, Faculty of Military Technology, University of Defence. His scientific activity is directed to the areas of sensor signal processing, analog circuits, software defined radio and avionics.

[26] W. Yao, Y. Yang, X. Wei, "Research on Coded Excitation Using Kasami Sequence in the Long Rail Detection Based on UGW", Electronics, vol. 11, no. 9, pp. 1-17, 2022, doi: 10.3390/electronics11091465.
[27] S. Chang, H. C. Wu, Y. Wu, X. Chen, "New probabilistic SINR analysis for capacity and reception-quality studies of DTV transmitter identification systems", Wireless Networks, vol. 28, no. 4, pp. 1521-1530, 2022, doi: 10.1007/s11276-021-02884-9.
[28] V. F. Yerokhin, O. V. Vakulenko, "Method of Selecting a Synchronization Preamble for Mutually Non-Orthogonal Digital Signals in Electronic Communication Systems with Random Multiple Access", Cybernetics and Systems Analysis, vol. 59, no. 4, pp. 640-650, 2023, doi: 10.1007/s10559-023-00599-7.
[29] Y. Wu, X. Wang, B. Caron, "Transmitter Identification Using Embedded Pseudorandom Sequences", IEEE Transactions on Broadcasting, vol. 50, no 3, pp. 244-252, 2004, doi: 10.1109/TBC.2004.834027.

Radek Bystřický was born in Plzeň, the Czech Republic in 1976. He received the M.Sc. degree in aviation electronics at the Military academy in 2001 and a Ph.D. degree at the University of Defence in Brno in 2009.

He studied from 2002 to 2003 at the ISAE-SUPAERO at Toulouse and from 2003 he is an assistant professor at the Department of Aviation Technology, Faculty of Military Technology, University of Defence. His research interest includes UAVs, sensor data processing, automatic flight control and inertial navigation systems.

Barbora Odvárková was born in 1998 in Mladá Boleslav. She received M.Sc. degree in Radar Technology and Electronic Warfare in 2022 from the University of Defence, Czech Republic. She is currently commander of group of soldiers at 532nd Electronic Warfare Battalion, Opava, Czech Army Ground Forces. Her research interests include radar technology, electronic warfare, electronic security systems, sensors and sensors signal processing.